Journal of Medicinal Chemistry

Article

Probing the ATP-binding pocket of protein kinase DYRK1A with benzothiazole fragment molecules

Ulli Rothweiler, Wenche Stensen, Bjorn-Olav Brandsdal, Johan Isaksson, Frederick Alan Leeson, Richard Alan Engh, and John S. Svendsen

J. Med. Chem., **Just Accepted Manuscript** • DOI: 10.1021/acs.jmedchem.6b01086 • Publication Date (Web): 13 Oct 2016

Just Accepted

ACS Publications

Journal of Medicinal Chemistry is published by the American Chemical Society. 1155 Sixteenth Street N.W., Washington, DC 20036

Probing the ATP-binding pocket of protein kinase DYRK1A with benzothiazole fragment molecules

Ulli Rothweiler[1,2], Wenche Stensen[2,4], Bjørn Olav Brandsdal[3], Johan Isaksson[4], Frederick Alan Leeson[2,4], Richard Alan Engh[1], John S. Mjøen Svendsen[2,4]*

[1]The Norwegian Structural Biology Centre, Department of Chemistry, UiT The Arctic University of Norway, N-9037 Tromsø, Norway,

[2]Pharmasum Therapeutics AS, Smørblomstvn. 36, N-9102 Kvaløysletta, Norway.

[3]The Centre of Theoretical and Computational Chemistry, Department of Chemistry, UiT The Arctic University of Norway, N-9037 Tromsø, Norway,

[4]Department of Chemistry, UiT The Arctic University of Norway, N-9037 Tromsø, Norway.

AUTHOR INFORMATION

*Corresponding author: john-sigurd.svendsen@uit.no

Keywords: Alzheimer's disease, DYRK1A, protein kinase, modeling, NMR, X-ray crystallography, inhibitor design, structure guided drug design

ABSTRACT

DYRK1A has emerged as a potential target for therapies of Alzheimer's disease using small molecules. Based on the observation of selective DYRK1A inhibition by firefly D-luciferin, we have explored static and dynamic structural properties of fragment sized variants of the benzothiazole scaffold with respect to DYRK1A using X-ray crystallography and NMR techniques. The compounds have excellent ligand efficiencies and show a remarkable diversity of binding modes in dynamic equilibrium. Binding geometries are determined in part by interactions often considered "weak", including "orthogonal multipolar" types represented by e.g. F-CO, sulfur-aromat, and halogen-aromat interactions, together with hydrogen bonds that are modulated by variation of electron withdrawing groups. These studies show how the benzothiazole scaffold is highly promising for the development of therapeutic DYRK1A inhibitors. In addition, the subtleties of the binding interactions, including dynamics, show how full structural studies are required to fully interpret the essential physical determinants of binding.

.

INTRODUCTION

Never in the history of man has the world's population been older. Advanced age has traditionally been regarded as a blessing, but a less welcome correlate of aging is dementia: rates of dementia rise sharply with age, with a prevalence of <5 % for populations younger than 65, and 15 – 40 % for those over 85.[1] Three out of four dementia patients have the dreaded Alzheimer's disease (AD),[1] first described in 1906 by the Bavarian neuropathologist Alois Alzheimer.[2] first described in 1906 by the Bavarian neuropathologist Alois Alzheimer.

In 1992 Hardy and Higgins presented the amyloid cascade hypothesis[3] to explain the molecular pathology of AD. The hypothesis posits that deposition of amyloid-β (Aβ) after secretase proteolysis of the amyloid precursor protein (APP) in the brain forms toxic insoluble fibrils (Aβ–plaques) that contribute to neuronal death and dementia. More recently, additional focus has been directed towards the role of the protein tau in AD.[4-10] Tau is a highly soluble protein that binds to and stabilizes microtubules in the axon of the nerve cells. In diseases where tau is involved in the pathology, hyperphosphorylation of tau prevents binding to microtubules, leading to inhibited axonal flow and thereby directly to neurodegeneration.[11,12] Hyperphosphorylated tau also self-assembles into aggregates that ultimately form the neurofibrillary tangles (NFTs)[13] initially observed by Alois Alzheimer himself as one of the histological hallmarks of AD.

The phosphorylation of protein tau in AD is a complex process whereby protein kinases such as GSK3β and CDK5/p25 play important roles. Recently it has been established that another protein kinase, DYRK1A, may play an even more central function, by orchestrating a wide variety of events that cause Alzheimer's disease.[14-16] DYRK1A can phosphorylate tau directly at the Thr212 site;[17] a process that inhibit the ability of tau to promote microtubule assembly, but also promotes additional tau phosphorylation by the protein kinase GSK3β,[4,18-20] which in turn increases tau hyperphosphorylation and subsequent loss of microtubule

stabilization further. In addition, DYRK1A phosphorylates the "alternate splicing factor" (ASF), leading to an increased amount of 3R tau relative to 4R tau, further facilitating tau aggregation.[16] DYRK1A also phosphorylates the "regulator of calcineurin" (RCAN), down-regulating calcineurin (Caln) phosphatase activity, thereby increasing levels of phosphorylated tau and reducing Caln/NFAT transcriptional activity.[21,22]

DYRK1A also plays important roles in amyloid plaque formation. DYRK1A increases secretase-mediated cleavage of APP into A peptides both via APP phosphorylation directly,[19,23] and by phosphorylation of presenelin 1 (PSEN1),[24] which even further increases secretase activity. Moreover, there is evidence that Aβ peptides stimulate DYRK1A expression in a positive feedback loop.[25]

The bulk of recent Alzheimer research has not only expanded the disease etiology from beta-amyloid plaques into tau and NFT's, but has also identified new potential targets for the development of therapeutic drugs, including the protein kinase DYRK1A.[26-28] There are however significant gaps in our knowledge of essential DYRK1A properties, including details of structure, plasticity, inhibitor binding potential and also critically biological consequences of activity modulation, before DYRK1A can be finally validated as a promising target for treatment of AD.

A significant proportion of the current literature has been concerned with identifying ligands that may inhibit DYRK1A, and a recent review summarizes the different chemotypes, all comprising Type 1 ligands that target the ATP-binding site.[15] We have recently discovered that luciferin and derivatives can act as selective DYRK1A inhibitors.[29] Little work however has surfaced that systematically explore the ATP-binding site of DYRK1A using a library of ligands. In the present study, a library of small benzothiazole fragment molecules was designed as ligands to systematically explore the repertoire of binding interactions between the ligand and the active site of the DYRK1A enzyme. In particular, hydrogen bonding

interaction and electronic effects are studied. The binding interactions between the ligands and the protein kinase were studied using a variety of biological, thermodynamic, structural and computational methods. The effectiveness of the ligands was measured in inhibition assays. Structural studies were performed by a combination of X-ray crystallography, dynamic NMR and computational simulations. Put together, these studies provide important new insights in potential interaction sites and design rules for *de novo* DYRK1A inhibitor construction.

RESULTS

Focused benzothiazole fragment library design

D-Luciferin and derivatives have recently been described as inhibitors of several protein kinases, particularly within the CMGC-family.[29] The inhibitory activity of the luciferin derivatives is in particular sensitive to modifications of the 6-hydroxy group on the benzothiazole system of luciferin, where O-methylation greatly diminishes inhibitory activity. Alterations in the dihydrothiazole ring of luciferin affects the inhibition of DYRK-family protein kinases only minimally. In the design of the current library it was decided to reduce the complexity of the luciferin ring system by replacing the dihydrothiazole moiety with a simple acetamide group, and greatly increase the repertoire of substituents in the benzothiazole ring, thus creating a focused fragment library design to explore the active site of DYRK kinases.

Choice of benzothiazole substituents

The substituents were selected according to their ability to donate or accept hydrogen bonds (or both) and their ability to affect the π-electron system in the aromatic benzothiazole ring system. All substituents chosen, with the exception of chloride and bromide, have hydrogen bond accepting properties varying from strong to weak. The hydroxyl group is the premier hydrogen bond donor (and/or acceptor) substituent, while the carboxamide moiety also has dual hydrogen-bonding capacities. The substituents have also been chosen to represent diversity in electronic effects spanning from activating to deactivating groups with predominantly mesomeric or inductive effects.

Geometry

The inhibitors were designed with the substituents placed in the 5- or 6-position ("end"-positions) of the benzothiazole nucleus, however, two fragments with either an hydroxy- or a

methoxy substituent in the 4-position ("edge-position") were also prepared. From the study on luciferin derived inhibitors[29] it was observed that the 4-hydroxy substituted analog occupied a region different from luciferin itself, so for the present study "end"-type were favored over "edge" type substitutions in order to address the same region of the protein kinase as luciferin. The 5- and 6-substituents are geometrically related through a pseudo 2-fold rotational axis that exchanges the positions of the sulfur and the nitrogen atoms in the thiazole ring (Figure 1). Besides this geometrical difference, properties that differ between equivalent 5- or 6-substituted molecules will also reflect differences of mesomeric or inductive effects. Substitution at the 5-position can influence the sulphur atom through mesomeric effects and the nitrogen atom through inductive effects, and vice versa for substitutions at the 6-position.

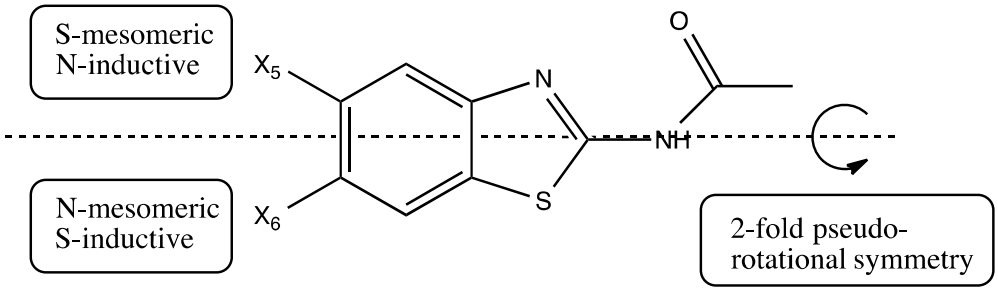

Figure 1. Design considerations for the benzothiazole library

Preparation of the inhibitors

The inhibitors of the library were prepared by microwave-assisted acetylation of the corresponding 2-aminobenzothiazoles. Several 2-aminobenzothiazoles are commercially available; those that were not were prepared by a modified two-step Stuckwisch procedure[30] according to Scheme 1. The 6-subsituted benzothiazoles were prepared from the corresponding *para*-anilines, analogously; the 4-substituted derivatives were prepared from the *ortho*-aniline. The *meta*-anilines can in principle give both 5- and 7-substituted benzothiazoles upon cyclization, however in practice, the 5-isomer dominates, and only in the

case of 3-trifluoromethylanisole substantial amounts of the 7-isomer was formed (the ratio between the 5- and 7-trifluoromethyl isomer was 65:35).

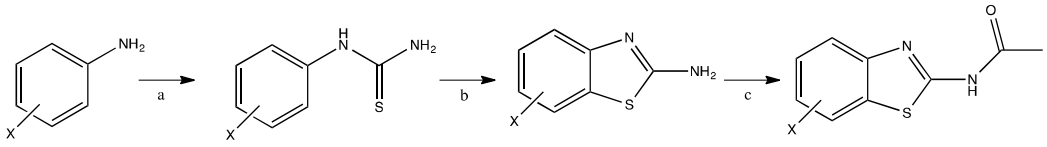

Scheme 1. a) NaSCN (1.5 eq.), TFA (2.5 eq.), Isopropyl acetate (reflux, 16h), b) Br_2 (1 eq.), LiBr (1.5 eq), AcOH, 40 °C, c) Acetic anhydride (2.2 eq.), DIPEA (3 eq.), DMF, Microvawe.

Protein kinase profiling

The protein kinase selectivity pattern was measured as a Gini coefficient[31] calculated on the basis of one of two kinase panels; either a large panel with 140 protein kinases or a smaller panel with 50 protein kinases (Table S1 lists the protein kinases included in the panels). The Gini coefficients is based on the Lorenz curve, which plots the proportion of the total inhibition of the full kinase panel that is cumulatively inhibited by each protein kinase. A Gini coefficient can thus vary from 0 (when all protein kinases are inhibited equally) to 1 (where the inhibitor inhibits only one protein kinase) and is regarded as a robust measure of kinase selectivity and is generally not greatly affected by panel size.[31] The fragments were profiled at a concentration of 100 μM to compensate for the expected low binding expected for fragments, and also to be able to pick up protein kinase targets with weaker binding affinity.

The results from the protein kinase profiling are presented in Table 1 as a Gini coefficient for each tested fragment molecule. With few exceptions, the observed Gini indices indicated that the fragments were quite selective (Gini index > 0.4). Members of the CMGC-superfamily (the DYRK-family, GSK3β, the CLK-family) as well as CK1 were among the targets commonly inhibited by the fragments.

The hydroxyl-substituted molecules **1** and **2** were more promiscuous inhibitors than the other members of the library. The halogen-substituted fragments were more selective, but the

highest selectivities were found for the methoxy-, trifluoromethoxy- and trifluoromethyl-compounds. There was also a clear trend that the 6-substituted molecules were less selective inhibitors than the corresponding 5-substituted molecules.

Inhibition of DYRK1A

The primary target for this study is the AD-relevant protein kinase DYRK1A. Inhibition of DYRK1A activity was measured as IC_{50} values determined using a radioactive filter-binding assay provided by the International Centre of Kinase Profiling at the University of Dundee, UK. The results are compiled in Table 1. The inhibitory activity of the fragment-like molecules ranged from 0.4 to 36.0 μM, corresponding to high ligand efficiencies (LE)[32] with LE values ranging from 0.369 – 0.600 kcal/mol per non-hydrogen atom. The most effective inhibitors were substituted with hydroxy or methoxy groups, halogen, or classical electron withdrawing groups (EWG) such as trifluoromethyl, cyano or nitro groups. In the majority of the molecules, the position of the substituent was also significant for inhibitory activity; for the hydroxy- and methoxy-compounds the 5-substituted compounds were 35 or 31 times more potent, respectively, than the 6-substituted isomers. A similar but weaker trend was observed for the 5-fluoro- and 5-bromobenzothiazoles that were 6 and 2 times more potent than the 6-substituted analogs, respectively. On the other hand, for other types of substituents, the 6-isomer was most effective; e.g. the 6-trifluoromethyl derivative was 24 times more efficient as a DYRK1A inhibitor than the 5-isomer. Despite low activity, the methyl derivatives showed a similar pattern with the 6-methyl derivative 4 times more potent than the 5-isomer.

Judged by the reported % residual activity against DYRK1A, the benzothiazole fragments in this work showed a similar level of inhibitory activity as D-luciferin.[29] However, both hydroxy- and methoxy-derivatives of the current molecules were potent DYRK1A inhibitors whereas methoxy-luciferin showed diminished activity relative to luciferin.[29]

Table 1. Inhibitory activity of benzothiazole derived fragments against protein kinase DYRK1A measured as residual activity (%) at an inhibitor concentration of 100 μM, IC_{50} values (μM) against DYRK1A, protein kinase selectivity calculated as a Gini coefficient profiled against a 50 member or a 140 member protein kinase panel at 100 μM and structure cluster as determined by X-ray crystallography.

Compound	X	% residual acitivity (DYRK1A)	IC_{50} (DYRK1A)	GINI coefficient	Structural cluster
1	6-OH	20	28.1	0.291	
2	5-OH	5	0.8	0.348	1
3	4-OH	25	35.0	0.489	
4	6-OCH_3	14	12.3	0.473	
5	5-OCH_3	2	0.4	0.618	1
6	4-OCH_3	15	10.5	0.668	
7	6-F	12	23.6	0.473	
8	5-F	7	3.9	0.527	1
9	6-Br	14	2.3	0.439	
10	5-Br	ND*	1.1	-	
11	6-Cl	6	2.9	0.475	2
12	6-CF_3	8	1.1	0.480	
13	5-CF_3	22	26.5	0.617	
14	6-CN	9	1.3	0.414	2
15	6-NO_2	6	0.7	0.500	2
16	6-$CONH_2$	ND*	15.7	-	
17	6-OCF_3	28	3.2	0.552	
18	6-CH_3	ND*	7.3	-	
19	5-CH_3	23	29.3	0.546	
20	H	43	36.0	0.551	

*ND: Not determined

Structure of the complexes

In the present work, six complexes between the benzothiazole fragment molecules and the DYRK1A protein could be successfully co-crystallized. The X-ray structures show the overall crystal packing to be similar to the DYRK1A structures previously published,[33,34] with tetramers (labeled monomer A, B, C and D) constituting the asymmetric unit. In general, the best electron density fit is found for monomer A. The greatest disorder is seen in monomer C, where especially the CMGC insert[35] shows a poor fit to the electron density (as indicated e.g. by low real space R-factors). In alignment with the previously described structures, several chains in the monomers show disulfide bridge formation between the HCD motif and the activation loop cysteine.[34] However, in approximately half of the monomers, the cysteine residues are reduced and/or in a mixed state, with additional evidence of radiation damage due to low amplitude electron density for cysteine C312. Nevertheless, the oxidation state of the cysteines C286 and C312 does not seem to influence the geometry of binding of the inhibitors.

The presence of the six inhibitors is clearly shown by omit difference density maps (Figure S1). However, the lack of strongly asymmetric features in the ligand, along with the degree of mesomery available to the inhibitors, creates ambiguity regarding binding poses for some inhibitors. Furthermore, the omit maps suggest that that there are binding poses in monomer D (and to a lesser degree B) that are not completely overlapping with the omit maps of the more densely packed monomer A (Figure S2).

The sulfur atom of the thiazole ring provides the strongest and usually unequivocal signal for interpretation of the difference density maps. Although the benzothiazole ring system is rigid, the acetamide moiety has two rotatable bonds with structural consequences for ligand-protein interactions. Both the bond linking the thiazole ring with the amide nitrogen atom and

the bond between the amide and the acetamide carbonyl are restricted to interconvertible torsional angles close to 0° and 180°. The first torsion can be defined by S1-C2-N(amide)-C(carbonyl) and be labeled *syn* (0° torsion angle) or *anti* (180° torsion angle), while the amide bond, defined by C2-N(amide)-C(carbonyl)-C(methyl) can be regarded as *trans* (180° torsion) or *cis* (0° torsion). The diffraction data do not resolve whether the amide torsion is *cis* or *trans*.

The six inhibitors can be subdivided into two structural clusters based on their poses in the ATP binding pocket. Cluster 1 inhibitors bind via hinge interactions with the 5-substitution moiety, while cluster 2 inhibitors bind "edge"-wise via hinge interactions with the benzothiazole and amide nitrogen atoms.

Structural Cluster 1

Cluster one comprises inhibitors **2**, **5** and **8,** with 5-OH, 5-OMe and 5-F substituents, respectively. The hydroxy-compound **2** can be placed in an unequivocally unique pose based on the thiazole sulfur atom and bind to DYRK1A with the 5-hydroxy group as the hinge binder, and the acetamide group forming H-bonds, either in a *syn-trans* conformation to the catalytic lysine K188 (Figure 2A), or alternatively in a *syn-cis* conformation to D307 from the DFG motif(dotted gray line in Figure 2A). Compound **2** can make two hydrogen bonds with the hinge, one with the hydroxyl oxygen as a hydrogen bond acceptor to the amide of L241, and one as a hydrogen donor to the carbonyl of L241. In comparison, the methoxy-compound **5** in crystallographic monomer A is slightly skewed inward into the lipophilic pocket forming the acetamido interactions to D307 in an *anti-cis* conformation (Figure 2B), whereas in crystallographic monomer D (Figure 2B'), the inhibitor shows an even larger inward skew, and the interactions between the acetamido moiety and D307 is now taking place through a *syn-cis* ligand conformation. The hinge interaction of compound **5** takes place through a hydrogen bond between the L241 amide and the methoxy-oxygen atom. Thus, in contrast to

the 5-hydroxy-compound **2**, where the hinge binding involves two hydrogen bonds, the methoxy-compound **5** can only form a single H-bond. The gray dashed line in Figure 2**A** represents an alternative H-bond to D307 when the inhibitor **2** binds with its alternate *syn*/*cis* isomer.

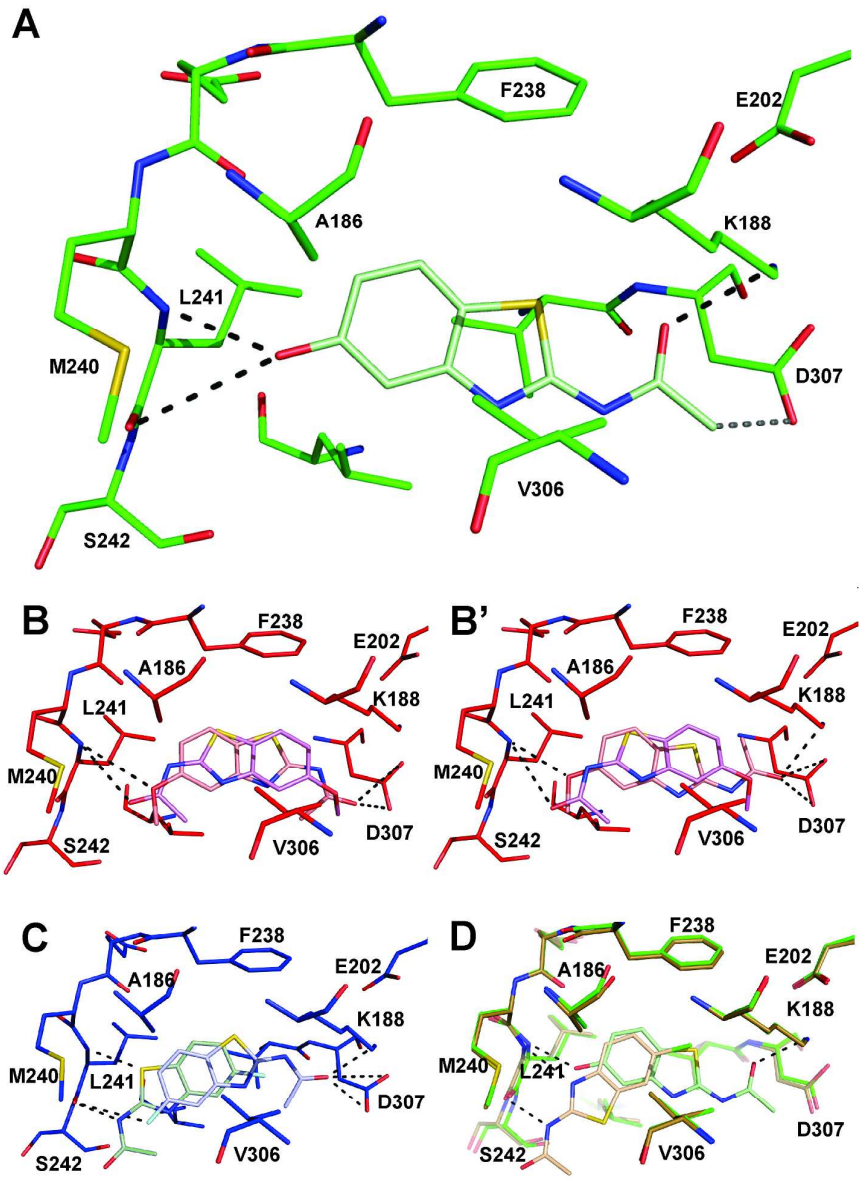

Figure 2. Binding poses of the individual inhibitors in the ATP pocket. **A**: 5-hydroxybenzothiazole **2** in its *syn*/*trans* conformation (dotted gray line represents the

interaction between the carbonyl oxygen and D307 in the alternative *syn*/*cis* conformation), **B**: Overlay of the two binding modes of 5-methoxybenzothiazole **5** in crystallographic monomer A, **B'**: Overlay of the two binding modes of 5-methoxybenzothiazole **5** in monomer D, **C**: Overlay of the two binding modes of 5-fluorobenzothiazole **8** in monomer A, **D**: Overlay of 6-chlorobenzothiazole **11** and 5-hydroxybenzothiazole **2**.

The 5-fluoro compound **8** also uses the substituent as a hinge binder, however through an unusual orthogonal multipolar interaction with a hinge carbonyl oxygen atom (Figure 2C).[36,37] The distance between C-F and O=C varies among the four fragments bound to the four chains A-D in the asymmetric unit, with distances between 3.1Å - 4.0 Å and an average of 3.6 Å. With the exception of the 4.0 Å distance, the fragments bind at distances typical for C-F···O=C interactions found in small molecule crystal structures[38] and protein ligand interactions.[36,37] Similar to the 5-methoxy-compound (in binding pose 1), the acetamide moiety of inhibitor **8** is anchored to the DYRK1A enzyme via a hydrogen bond to both D307 and K188 in an *anti*/*cis* acetamide conformation.

Additional binding poses in Cluster 1

For the methoxy-compound **5,** the difference electron density map also reveals an additional sulfur position corresponding to a binding mode where the inhibitor is rotated by 180 degrees around its short axis, effectively swapping the positions of the acetamide carbonyl oxygen atom and the methoxy oxygen atom compared with the principal binding pose (Figure 2B and B'). In the alternate binding mode the L241 amide forms a H-bond to the *anti*/*cis* acetamide carbonyl oxygen. Away from the hinge, 5-methoxy group is oriented towards the catalytic lysine K188, which remains ordered and hydrogen bonded to its active state partner E203 from helix C. The distance between the methoxy-oxygen atom and the terminal amine

nitrogen of K188 is ~4 Å, too far for a hydrogen bond, but clearly an important local electrostatic interaction.

In all binding poses identified so far the ligand orients its thiazole sulfur atom towards the gatekeeper phenylalanine, forming a sulfur-aromat interaction. The thiazole sulfur–phenylalanine phenyl distance varies among the inhibitors, and the shortest distance to the phenyl ring (3.5 Å) is found for the 5-fluoro inhibitor **8**, while the other two inhibitors show distances that range between 3.9 and 4.5 Å.

In monomer A of the crystallographic tetramer of the compound **8** complex, the 5-fluoro compound can also adopt a binding pose atypical for Cluster 1. The electron density for 5-fluoro molecule **8** in monomer A of pdb code 5A4L is consistent with two distinct poses, and both poses are present in monomer A (Figure S1C). In the alternate binding pose (Figure 2C) the 5-fluoro inhibitor is oriented along the hinge with the thiazole sulfur atom oriented towards L241, and a hydrogen bond linking the amide of S242 and the acetamide carbonyl, which is in an *anti*-conformation. The distance between the thiazole sulfur atom and the L241 nitrogen atom is 3.1 Å, suggestive of a hydrogen bond. In the alternate binding pose the fluorine atom is located in a similar position as occupied by the sulfur atom in the normal binding pose (Figure 2C), however the distances between the fluorine atom and the carbon atoms in the phenyl ring are between 5.2 and 6.0 Å, too long for a specific fluorine-aromat interaction. The finding, however, that the binding poses of compound **5** in the B, C and D monomers of the asymmetric unit are unambiguously aligned with the normal Cluster 1 binding mode indicates that the alternate binding pose found only in monomer A is a less preferred binding pose for the 5-fluoro inhibitor.

Structural Cluster 2

Cluster two (represented in Figure 2D by the 6-chloro-inhibitor **11**), contains the binding poses adopted by benzothiazoles with 6-chloro-, 6-nitro- and 6-cyano-substituents (**11**, **14** and **15**). The binding poses of Cluster 2 are uniquely identified by the thiazole sulfur atom and the substituent in the 6-position, and show the thiazole- and acetamide-nitrogen atoms to bind at the hinge (the thiazole nitrogen atom to the L241 amide and the acetamide nitrogen to L241 carbonyl moiety), while the substituents are oriented toward the gatekeeper F238 as shown for compound **11** in Figure 2D. All inhibitors in structural cluster two bind with the acetamido group in the *syn*-conformation required for the second hydrogen bond to L241, but the acetamide carbonyl group is not involved in any hydrogen bond formation. The 6-chloro-substituent of fragment **11** superimposes with the thiazole sulfur atom of the 5-hydroxy-substituted fragment **2** (Figure 2D) replacing the sulfur – aromat with a halogen – aromat interaction. The chlorine atom in **11** interacts with F238 via one edge of the aromatic ring system. While the distance to the center of the aromatic π system is approximately 4.4 Å, the closest contact to the phenyl ring edge is only 3.6 Å. These distances are in agreement with typical halogen phenyl interactions.[37,39] The angle between the plane of the aromatic ring and the chlorine atom is around 80°. Thus in this case the chlorine atom interacts with the π system itself rather than forming the more common CH···Cl interaction.[37] Similar interactions of the substituent with the π-system of the gatekeeper residue can be observed for 6-cyano- (**14**) and 6-nitro-benzothiazole (**15**). The 6-cyano-group is nearly parallel to the edge of the phenylalanine, at a distance of ~4.2 Å. The 6-nitro-compound **15** participates in a nitro-π-stacking interaction. One of the oxygen atoms in the 6-nitro-substituent is placed below the center of the π system at a distance of 3.3 Å; the nitrogen itself is at a distance of 4.3 Å. The substituents of the inhibitors in structural cluster two do not form hydrogen bonds to D307

nor to the catalytic lysine K188, which is ordered and hydrogen bonded to its partner E203 from helix C.

Dynamics of ligand binding

The X-ray structure shows that the 5-methoxy-compound **5** probably binds to the active site of DYRK1A in either of two distinct binding poses related by a 180° rotation about an axis perpendicular to the benzothiazole ring (Figure 2B). To further probe this structural ambiguity, the binding mode of **5** was investigated using NMR techniques. A slight line broadening of the ^{1}H-signals of ligand **5** was observed in the presence of DYRK1A (100:1 ligand:protein in D_2O) (Figure S3), characteristic of a rapid equilibrium between bound and unbound states, consistent with the low μM binding constant. The presence of rapid binding equilibrium between free and protein bound ligand was further corroborated in a Saturation Transfer Difference (STD) experiment (Figure S4).

The multiple binding modes of **5** to DYRK1A were examined by a 2D transferred NOE (trNOESY) experiment on the same sample as above. The trNOESY experiment revealed an unexpected long-range correlation between the methyl group of the acetamide moiety and the H-6 hydrogen of the benzothiazole ring (Figure S5A). This correlation disappears in an experiment performed in the absence of protein, showing directly that compound **5** interacts with the DYRK1A protein in two distinct binding poses. The correlation arises when the H-6 atom of the benzothiazole ring in one binding mode occupies the same space in the protein as the acetamide methyl group in the alternate binding mode (corresponding to a 180° flip of the ligand between the binding poses). This observation is fully consistent with the two binding modes proposed by the X-ray crystallographic data (Figures 2B and B') existing in rapid equilibrium on the mixing time scale (milliseconds). Lacking a better term, this will be referred to as "molecular auto-correlation" in the discussion below – *i.e.* there is a correlation

between the position of one proton with the position of another proton in the same molecule at an earlier point in time.

The binding mode of the 5-hydroxy-ligand, **2** to DYRK1a was also investigated by trNOESY. The experiment revealed a weak "auto-correlation" between the acetamido methyl group and the H-4 hydrogen at the benzothiazole moiety (Figure S6). As with compound **5**, this correlation is consistent with two binding poses related by a 180° flip between the binding modes, however for the hydroxyl compound **2**, one pose is significantly more populated than the other. X-ray crystallography showed only a single well-resolved binding mode for **2**. Interestingly, while the 5-hydroxy compound **2** shows an "auto-correlation" between methyl-3' and H-4, the methoxy compound **5** instead shows a correlation between methyl-3' and H-6, indicating that the binding modes of ligands **2** and **5** are slightly different. This observation is consistent with the binding modes in the X-ray structures for **5** (monomer D) and **2** (Figures 2B/B' and 2A, respectively) where compound **5** is slightly more skewed inward than compound **2**.

MD simulations were carried out for compound **2** and **5** in two binding modes to determine the relative binding affinities of the respective binding modes observed in X-ray and NMR structures. Consistent with the experimental data, the free energy simulations show that the difference in binding free energy between the two orientations of compound **2** is 2.4±0.4 kcal/mol in favor of the X-ray conformation. For compound 5, the binding free energy difference between the two orientations is 0.7±0.3 kcal/mol, indicating that the two modes are equally populated.

A trNOE competition experiment between ligands **2** and **5** further revealed that the 5-methoxy group in ligand **5** displayed interligand trNOEs (ILOE) to the aromatic 4-, 6-, and 7-hydrogens of the hydroxy ligand, **2**, implying that the dominant binding orientations of **2** and **5** are opposite (Figure S7). As ligand **5** binds to DYRK1A with two significantly populated

binding modes, correlations from the near overlapping acetamide methyls of **2** and **5** produced ILOe's to the H-6 and H-7 hydrogen of **2** and the H-4 and H7 of **5** .

Because the acetamido methyl groups of compound **2** and **5** were insufficiently resolved in the 2D trNOESY experiment, an additional 1D dpfgse-NOESY experiment with higher ^{1}H resolution was performed. Selective irradiation of the methoxy group in **5** produced a clear ILOE to the acetamido methyl group in ligand **2,** in addition to an "auto-correlation" to its own acetamido methyl group (Figure S8).

The findings from the trNOE competition experiments of ligands **2** and **5** are in good agreement with the results obtained by X-ray crystallography. Ligand **5** binds in two well populated different poses differing by a 180° flip, whereas ligand **2** predominantly binds in one binding pose similar, but slightly skewed compared to one of the binding poses of **5** (Figure 2 A, B and B').

A similar trNOE competition experiment was also performed between the 5-hydroxy (**2**) and 6-hydroxy (**1**) ligands (Figures S9). In this case the ILOE's are edge to edge pseudo-contacts between the aromatic protons, a finding that implies that **1** and **2** bind in similar poses, where the hydroxyl- and the acetamido groups occupy the same space, respectively, but the benzothiazole ring of **1** is flipped around its long axis, allowing the 6-hydroxyl groups to occupy the same space as the 5-hydroxyl group in **2**. As a consequence of the benzothiazole swap, compound **1** binds to DYRK1A with the sulfur atom facing the outside of the active site while compounds **2** and **5** bind with their sulfur atom facing inward in the active site in all their binding modes.

DISCUSSION

From the finding that luciferin acts as an inhibitor of DYRK1A as well as other members of the CMGC-superfamily (the DYRK-family, GSK3β, the CLK-family) as well as CK1, a 20 member focused fragment library based on the benzothiazole scaffold was designed, prepared, profiled and tested for inhibitory activity against DYRK1A. The results showed that several members of this library displayed high DYRK1A selectivity (with GINI indices > 0.500) and very high binding efficacy (LE up to 0.600 kcal/mol). Furthermore, clear trends in fragment structure-DYRK1A inhibitory activity and fragment structure-protein kinase selectivity could be discerned.

With two exceptions, the 4-hydroxy and the 4-methoxy isomers (compounds **3** and **6**) respectively) that both showed weak inhibitory activity against DYRK1A, the benzothiazole fragments were designed to be pseudo-symmetrical, i.e. the 5- and 6-substituents are related by a 180° rotation along the long molecular axis, effectively swapping the positions of the thiazole N- and S-atoms (Figure 1). Despite the pseudosymmetric nature of the fragments, large regioisomeric differences in the inhibitory activities against DYRK1A (determined as IC50 values) could be observed (Table 1). Inspection of Table 1 reveals that the 5- and 6-substituted fragments could be classified according to their activity, strong (< 5 μM) vs weak (> 5 μM), and regional selectivity (activity of 5-isomer vs the corresponding 6-isomer). Based on these criteria, four classes of inhibitors can conveniently be constructed. The first class consists of the fragments where substitution in the 5-position produces more effective inhibitors than the corresponding substitution in the 6-position with a high degree of selectivity (> 5 times). Class 1 consisted of inhibitors with methoxy-, hydroxy- and fluoro-substituents, and the regional selectivity was up to 35 fold for the hydroxyl-substituent. The second class consisted of the bromo-substututed benzothiazoles (**9** and **10**) where both isomers produced strong inhibitors (albeit with a weak preference for the 5-isomer). The third

class contained compounds where substitution in the 6-position produced strong inhibitors. Class three consists of compounds with chloro, cyano, nitro, trifluoromethoxy and trifluoromethyl substituents. For the fragments with a trifluoromethyl-substituent (compounds **12** and **13**), the 6-isomer was 24 times more potent than the 5-isomer. The last class consisted of inhibitors with weaker activity against DYRK1A (unsubstituted benzothiazole as well as carboxamido and methyl substituted benzothiazole derived fragments), although some selectivity (towards the 6-position) for the methyl substituted isomers was evident.

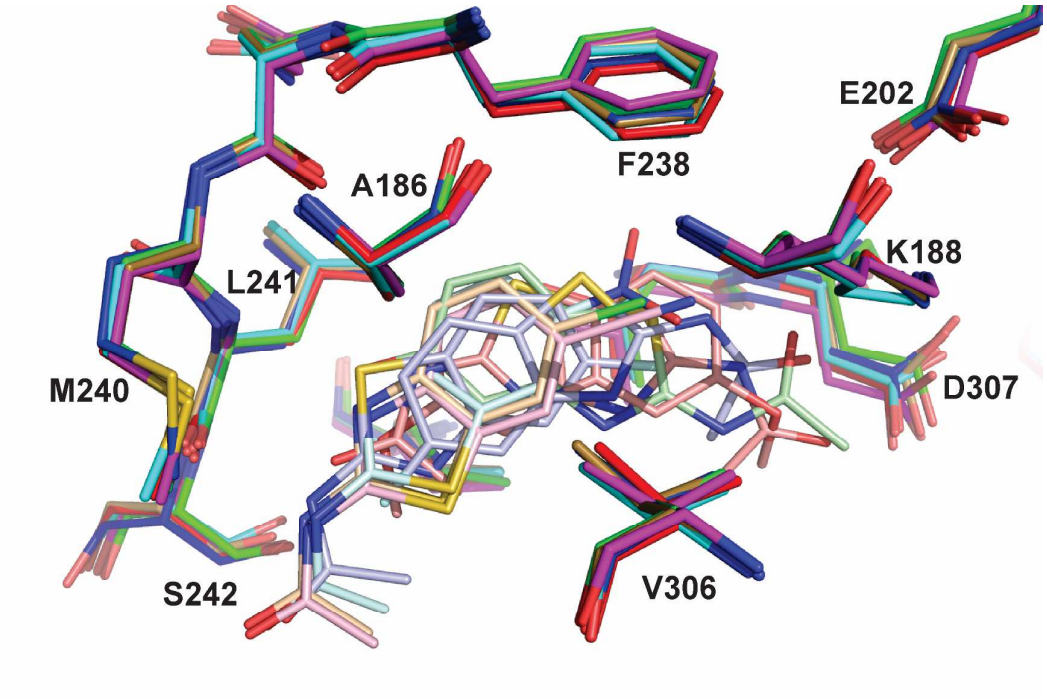

Figure 3. Overlay of all binding poses from the X-ray crystallographic structures for the DYRK1A complexes with compounds **2**, **5**, **8**, **11**, **14** and **15**.

The X-ray and NMR structural studies reveal that the present benzothiazole fragment library quite extensively explores the ATP-binding pocket. This is depicted in Figure 3 which shows a superposition of all binding poses observed in the X-ray crystallography structures. The effective exploration of the binding pocket also allows many of the trends in structure – DYRK1A inhibitory activity to be understood and interpreted from the X-ray crystallographic

and NMR structural studies of the target-ligand complexes. Furthermore, the X-ray studies also suggest that some ligands may bind in different binding poses, a feature confirmed by the transient NOE NMR experiments.

A

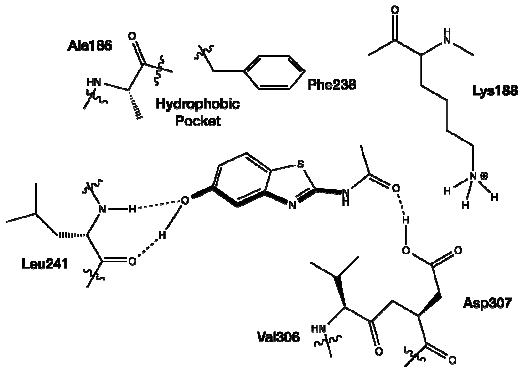

B

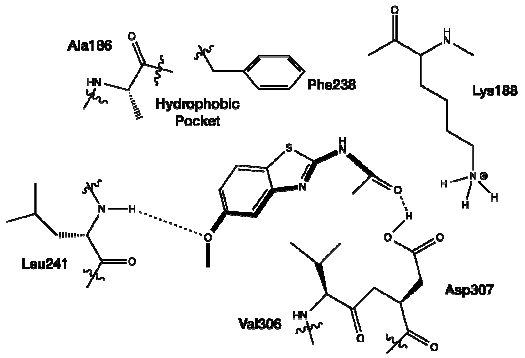

C

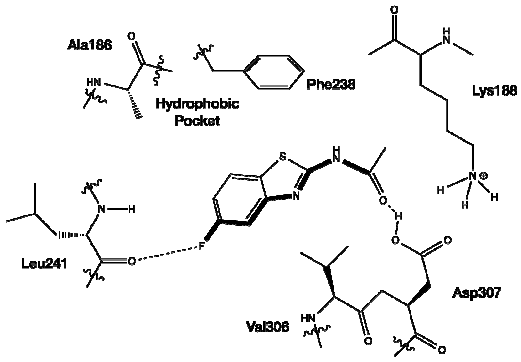

D

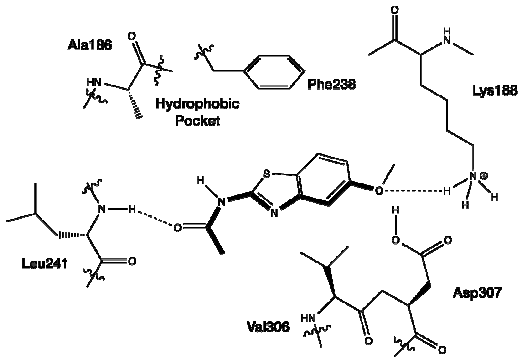

E

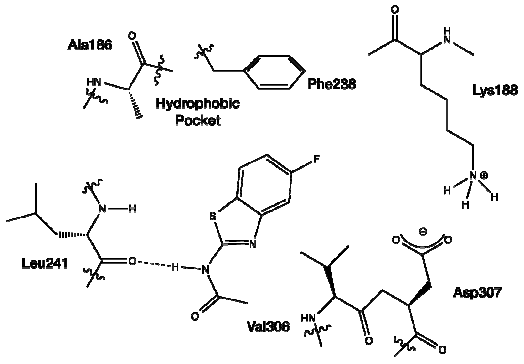

F

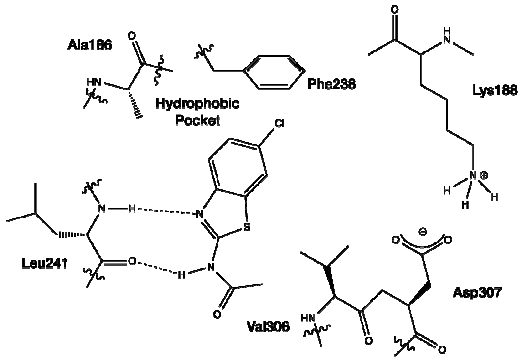

Figure 4. Schematic representations of the binding poses for representative members in Cluster 1 and Cluster 2. Panel A shows the 5-hydroxy-compound **2**, Panels B and D shows the two alternative binding poses of the 5-methoxy-compound **5**, Panels C and E shows two binding poses of the 5-fluoro-compound **8**, and Panel F shows the binding pose of the 6-chloro-compound **11** as an example of the binding mode in Cluster 2.

The X-ray crystal structures fall broadly into two clusters; the first cluster consists of the Class 1-inhibitors with high positional selectivity for the 5- position. These are represented in the X-ray structures with the 5-hydroxy derivative **2**, the 5-methoxy-derivative **5** and the 5-fluoro-derivative **8**. The overall position of the inhibitors from this cluster in the active site of DYRK1A is determined by the interactions between the 5-substituent to the hinge residue L241 and the acetamide moiety to the D307 from the DFG motif or K188, as illustrated in Figure 4A-C. The 5-F compound **8** is able to form a C=O···F bond with a geometry suitable for productive "orthogonal multipolar interactions" to the hinge L241. This interaction, however, is weak compared to the hydrogen bonds seen for the 5-OH and 5-OMe compounds; as a consequence, the 5-F fragment shows a 5-fold reduction in affinity compared to the other two.

Noteworthy for the Cluster 1 X-ray structures is the presence of a second binding pose defined by a flip about the short axis for the 5-OMe compound, switching the hinge binding interaction from the methoxy group to the acetamide carbonyl (e.g. Figure 4B vs. Figure 4D). This second binding pose for compound **5** is confirmed by the trNOE experiments. The trNOE NMR also indicates that this flip along the short axis is possible for the 5-OH compound **2** as well, however, the alternate binding pose in compound **2** is much less populated in the trNOE experiments, and is not observed in the X-ray structure, showing that the hydroxyl group at the hinge with the potential of two hydrogen bonds is clearly preferred

compared to the alternate binding pose with its single hydrogen acceptor (the carboxamide carbonyl group).

A significant feature of all X-ray and NMR structures of these two binding poses is that the thiazole sulfur atom is oriented towards the interior of the ATP binding pocket in an interaction with the gatekeeper phenylalanine F238. The distance between the thiazole sulfur atom and the face of the F238 phenyl group varies between 3.5 and 4.5 Å, compatible with favorable sulfur – π interaction energies.[40] Due to the pseudorotational relationship between the 5-substituted and the corresponding 6-substituted inhibitors, the 6-substituted isomers could adopt the same hinge and acetamido-D307/K188 interactions as the 5-isomers; however, the 6-isomers would then have to orient the thiazole nitrogen atom towards the inside of the pocket and not the thiazole sulfur. This allows the conclusion that the regional selectivity for the 5-isomers of the Class 1 inhibitors is to a large degree attributable to the thiazole sulfur – gatekeeper phenylalanine interaction.

A direct insight into the importance of the sulfur – aromat interaction is provided by trNOE NMR competition experiments of the 5-hydroxy fragment **2** and the 6-hydroxy fragment **1**. The experiments show that the hydroxyl groups of **1** and **2** occupy the same space of DYRK1A, just as their acetamido groups do. This finding illustrates the governing influence of the hinge and D307 interactions on the overall binding pose of these fragments. However as discussed above, the 5-hydroxy compound **2** is bound with its thiazole sulfur facing the phenyl group of F238, whereas the same binding pose in **1** would leave the thiazole sulfur atom exposed to the solvent. The influence of sulfur-aromat interaction is thus evident when comparing the inhibitory activities of **1** and **2** (Table 1), where the IC_{50} value of compound **2** is 35 times lower than for compound **1**. A similar interaction pattern for the methoxy-substituted pair **4** and **5** can also explain the 30-fold difference favoring the 5-methoxy-compound. The fluoro-substituted compounds bind less efficiently (the 5-fluoro-compound **8**

inhibits 10 times less efficiently than the 5-methoxy-compound **11**), resulting from the weaker orthogonal multipolar interaction linking the fluorine atom to the carbonyl of L241. However, only the 5-fluoro-isomer is capable of a sulfur – aromat interaction with F238, as described above, leading to an expected regioisomeric selectivity for the 5-isomer. The observed selectivity is only 6-fold and is thus not as prominent as for the hydroxyl and methoxy substituted compounds. However, because the 5-fluoro-compound displays a binding mode along the hinge (Figure 4E) with a moderate strength hydrogen bond to the thiazole sulfur, the 6-isomer may as well adopt a similar binding mode, decreasing the sensitivity to the regioisomeric differences in the overall orientation of the benzothiazole ring system.

Structural cluster two consists of the Class 3 fragment molecules with classical electron withdrawing substituents in the 6-position, including nitro- (**14**) and cyano-groups (**15**), as well as a chlorine substituent (compound **11**) with a combined inductive withdrawing, but mesomeric electron donating ability. The structures within cluster two are very similar to each other as depicted in Figure 4F, but are very different from the structures in cluster one. The binding mode in cluster two is most likely governed by the electron withdrawing ability of the 6-substituent that is directed towards the gatekeeper phenylalanine, allowing the formation of a σ-hole – π interaction[37] (for the 6-chloro inhibitor **11**), a nitro-π interaction (for the 6-nitro inhibitor **14**) or a π – π interaction (for the 6-cyano inhibitor **15**) between the substituent and the aromatic ring system of F238. The amide group of the acetamide moiety forms a hydrogen bond to the carbonyl group of L241. Furthermore, close contacts ranging from 3.1 Å (for the 6-chloro derivative) to 3.3 Å for the (6-cyano and 6-nitro derivatives) between the amide nitrogen of L241 and the nitrogen atom of the thiazole ring are observed. These distances correspond to hydrogen bonds, either "moderate and mostly electrostatic" or "weak, electrostatic" according to the definition of Jeffrey.[41] The mesomeric electron withdrawing effect coupling the 6-substituent directly to the thiazole nitrogen atom through resonance

would be expected to weaken the hydrogen bond acceptor ability for the thiazole nitrogen atom relative to the corresponding 5-isomer, or to compounds with a mesomeric electron donating 6-substituent, hence the observed binding mode is surprising, and highlights the importance of the "weak" interaction between the electron withdrawing 6-substituent and the gatekeeper Phe238.

The bromine substituted compounds **9** and **10** take an intermediate position, where both the 5- and the 6-isomer show substantial inhibition. It is not unreasonable to expect that the 6-bromo compound would binds to DYRK1A with a pose similar to that of the 6-chloro compound **11**. The main interactions in the binding of **11** would thus be a hydrogen bond between the acetamido-NH and the carbonyl of L241, as well as a halogen σ-hole π-interaction with F238, and a weak hydrogen bond between the L241 amide and the thiazole-nitrogen atom. If bound in the same pose, the 5-bromo-isomer would be able to enjoy the same strong interactions as the 6-isomer (i.e. σ-hole π-interaction and the acetamide hydrogen bond), but would replace the weak thiazole-nitrogen hydrogen bond with a weak thiazole sulfur hydrogen bond. The 5-bromo position is preferred, but the difference in IC_{50} values (two-fold) between the 5- and 6-bromo isomers is marginal compared to the other cases where a clear regiochemical trend is observed.

The protein kinase inhibition promiscuity of the studied inhibitors expressed as Gini-coefficients was also influenced by the type and regiochemistry of the benzothiazole substituent. Generally, the inhibitors in the library showed high selectivity for DYRK1A, with Gini-indices above 0.500. On the other hand, some of the strong inhibitors, in particular the hydroxyl-substituted fragments **1** and **2**, were much less selective for DYRK1A than the other members of the library. The kinase selectivity is significantly higher for the halogen-substituted fragments, and highest for the methoxy-, trifluoromethoxy- and trifluoromethyl-substituted fragments. There is also a clear trend that substitutions in the 6-position of the

fragments gives less selective inhibition than fragments with substituents in the 5-position. The profiling data, performed at a ligand concentration of 100 μM, indeed, reveals that the hydroxy compounds are more promiscuous than the other members of the fragment library, inhibiting an array of protein kinases at a moderate level. The reason for this difference in promiscuity is likely related to the dual hydrogen bond donor acceptor properties of the phenolic hydroxyl group that provide generic hinge-binding properties to the hydroxy-compounds **1** and **2**. It is important to note that the 5-isomer **2** is an effective DYRK1A inhibitor, whereas the 6-isomer **1** is not. The present structural studies show that the difference can be attributed to the additional binding interaction between the thiazole sulfur atom and the gatekeeper phenylalanine residue. The 5-isomers of methoxy- and the fluoro-substituted compounds are far more selective DYRK1A inhibitors, in large part because their "generic" hinge binding capacity is substantially lower than that for the 5-hydroxy-compound **2**, and thus are more dependent on more specific kinase interactions. The major difference in protein kinase profiles between the 5-methoxy- and the 6-methoxy-isomer is that the 5-isomer inhibits DYRK1A particularly well, whereas the profile outside the DYRK family is rather similar for both compounds. The sulfur – aromat interaction is thus not only responsible for higher binding affinities, but also for the higher 5-isomer selectivity of these compounds. For the 6-isomer selective compounds with electron withdrawing substituents, profiling data are available only for the trifluoromethyl-substituted compounds **12** and **13**. These compounds belongs to the structural class for which the interaction between the ligand and DYRK1A takes place via two hydrogen bonds; one between the acetamide-H atom and a hinge carbonyl, the other between a hinge amide and the thiazole nitrogen atom. This interaction is complemented by interactions between the electron withdrawing substituent and the gatekeeper phenylalanine. The 5-trifluoromethyl compound **13** is a modest DYRK1A inhibitor, but is a selective inhibitor for the PIM1 and PIM3 kinases.

CONCLUSION

The protein kinase DYRK1A has emerged as a potential target for small molecule therapy of Alzheimer's disease. In the present study we have explored static and dynamic structural properties of fragment sized variants of the benzothiazole scaffold with respect to DYRK1A using X-ray crystallography and NMR techniques. Not only do several of these small inhibitors have excellent ligand efficiencies, their DYRK1A complex structures show a remarkable diversity of binding modes in dynamic equilibrium. Our studies have shown that the overall binding modes of these fragment-sized inhibitors are mainly determined by classical interactions such as hydrogen bonding and electrostatic interactions. However, the detailed binding geometries are apparently driven by additional types of interactions often considered "weak", including "orthogonal multipolar interactions", e.g. F-CO, sulfur-aromat, halogen-aromat. The most stable binding mode or modes in equilibrium are determined by the sum of these interactions, together with the effects of electron withdrawing groups that modulate hydrogen-bonding propensities, but without taking the "weak" interactions into account no reliable model for structure activity relationship (SAR) can be derived. Furthermore, several of the small benzothiazole inhibitors display dynamic behavior by binding in multiple binding poses in rapid (NMR-time scale) exchange, a feature that adds a further layer of complexity to the SAR model. On the other hand, by taking both the detailed structural interactions and the dynamic behavior into account a reliable SAR model of DYRK1A inhibition by small, fragment sized, benzothiazole inhibitors can be derived, a model which can even provide insight into protein kinase selectivity. The present work shows that even fragment-sized benzothiazole derivatives can be effective and selective inhibitors of the protein kinase DYRK1A, however, the fragment nature of the compounds would require significant effort in translating the molecules into drug lead compounds. On the other hand,

the identification of multiple "weak" binding interactions in addition to the classical hinge and conserved lysine interactions provides guidance for further optimization. In particular, the interactions with the gatekeeper F238 residue of DYRK1A may be modulated by design for enhancing both potency and selectivity for future inhibitors.

Furthermore, the present study also illustrates the benefit of combining "static" X-ray structural determination with "dynamic"-NMR experiments for a more comprehensive understanding of fragment binding, providing a foundation for the SBDD effort to prepare selective and effective DYRK1A inhibitors that is underway in our laboratories.

EXPERIMENTAL SECTION

Instrumentation and chemicals

All the chemicals and solvents were supplied by Merck or Sigma-Aldrich and used without further purification. NMR spectra were acquired on an Agilent inova spectrometer operating at 600 MHz for 1H equipped with an inverse cryogenically enhanced HCN probe (2nd generation). High resolution mass spectra were recorded on a Thermo Scientific Orbitrap mass spectrometer using electrospray ionization.

Protein production and crystallization

The kinase domain of DYRK1A (residues 126–490) was produced in bacteria as a HIS-tagged fusion protein and purified as described in detail by Alexeeva et al.[34]

Co-crystallization with the inhibitors followed the protocol described by Alexeeva et al.[34] The kinase DYRK1A was concentrated to 7–10 mg/ml and mixed with inhibitor solutions in DMSO, to achieve an approximately 10-50 fold molar excess of the inhibitors. The crystallization solution [100 mM potassium thiocyanate, 50-100 mM NaCl or KCl, 10-16% PEG 3350] gave octahedron-shaped crystals within 5–7 days at room temperature. Crystals were cryoprotected in crystallization solution modified to include 30% ethylene glycol and were flash-cooled in liquid nitrogen.

Structure solution and refinement

X-ray diffraction data were collected at the Helmholz Zentrum Berlin (Berlin Electron Storage Ring Society for Synchrotron BESSY II), Germany and the European Synchrotron Radiation Facility ESRF ID29, Grenoble, France. The images were integrated using the XDSapp software[42] (for the structures from BESSY II) and XDS[43] for the structure from ESRF. The structures were solved by molecular replacement with Phaser[44] using the DYRK1A structure with PDB code 4NCT[34] as search model. The structures were refined by iterative cycles of PHENIX[45] and the CCP4[46] program REFMAC5[47] followed by the manual

refitting of residues and inhibitors into the electron-density between the refinement cycles and placement of water molecules using Coot v.0.7.2.[48] PRODRG[49] was used to generate the cif files for inhibitors. The crystallographic data and model statistics are summarized in Table S2.

NMR

All NMR spectra for probing DYRK-inhibitor interactions were acquired in 90:10 D2O:DMSO-d_6 to assist inhibitor solubility with the inhibitors in 100:1 excess relative to DYRK1A (1 mM:10μM). For INPHARMA-type trNOESY, typically 2048x200 complex points were acquired in 64 transients at mixing times of 30-300 ms with presaturation on the HDO signal during the relaxation delay. Saturation Transfer Difference spectra were acquired using 2.5 s gauss shape saturation at 1.15 ppm as the 'on' frequency and 29.6 ppm as the 'off' frequency. Solvent signals were suppressed by presaturation and excitation sculpting, and the protein signal was suppressed by a 10 ms spinlock.

All trNOESY experiments were acquired with- and without the presence of protein to rule out direct ligand-ligand interactions in solution, or solvent-relayed transfer.

Measurement of protein kinase inhibition

The determination of protein kinase inhibition was performed at the International Centre for Kinase Profiling at the University of Dundee, U.K. The method used is a radioactive filter binding assay using ^{33}P ATP. The ATP concentrations were at or below the calculated Km for ATP for each particular kinase.[50,51]

General synthetic procedures

Preparation of 2-Aminobenzo[d]thiazoles

Preparation of thiourea derivatives. The aniline derivative (1 eq) was added to a mixture of NaSCN (1,5 eq) in isopropylacetate (1 mL/mmol aniline) before addition of trifluoroacetic

acid (2,5 eq). The reaction mixture was refluxed for 16 hours. The crude product was isolated by triturating with water.

Cyclization of thiourea derivatives. The thiourea derivative above (1 eq) was dissolved in acetic acid (2 mL/eq thiourea) and LiBr (1.5 eq) was added. Bromine (1 eqv) was added in portions and the reaction mixture was heated to 40 ^{O}C. The crude product was isolated by filtration and washed with Na_2CO_3 solution and water before drying.

Acetylation of 2-aminobenzo[d]thiazoles

The 2-aminobenzothiazole (1 eq) and acetic anhydride (2.2 eq) were dissolved in of DMF (4 mL/eq benzothiazole). DIPEA (3 eq) was added before microwave irradiation at 60^{O}C for 2 h. The reaction mixture was triturated into $NaHSO_4$ solution before the crude product was isolated by filtration. The 2-aminobenzo[d]thiazoles were purified either by crystallization or by using reversed-phase HPLC on a Delta-Pak (Waters) C_{18} column (100 Å, 15 μm, 25 × 100 mm) with a mixture of water and acetonitrile (both containing 0.1% TFA) as eluent. The purity of the final products was further analyzed by reversed phase-HPLC using an analytical Delta-Pak (Waters) C_{18} column (100 Å, 5 μm, 3.9 × 150 mm) and the products were more than 95% pure.

ANCILLARY INFORMATION

Supplementary information

Listing of protein kinases used in the panel screening. Synthesis details and spectroscopic data for compounds prepared for this study. X- ray data collection and refinement statistics and omit maps for the binding pockets. NMR spectra (Saturation transfer difference, trNOESY and 1D dpfgse NOESY) of compounds 1, 2 and 5 in the presence of DYRK1A. Computational details.

Accession codes

PDB ID DYRK1A complexes: Compound **2**, 5A3X; compound **5**, 5A4E; compound **8**, 5A4L; compound **11**, 5A4Q; compound **14**, 5A4T; compound **15**, 5A54.

Notes

UR, WS, FAL and JSMS are employees of Pharmasum Therapeutics AS. The authors declare no competing interests.

Acknowledgment

The present work has been financially supported by Pharmasum Therapeutics AS of Tromsø, Norway and the Norwegian Research Council (grant no. ES546707).

Abbreviations

DYRK1A, dual-specificity tyrosine phosphorylation-regulated kinase 1A; GSK3β, Glycogen synthase kinase 3 beta; CK1, casein kinase 1; PIM1, Proto-oncogene serine/threonine-protein kinase 1; PIM3, Proto-oncogene serine/threonine-protein kinase 3; trNOE, transient nuclear Overhauser effect; 1D dpfgse NOESY, One-dimensional double pulsed field gradient spin echo nuclear Overhauser effect spectroscopy.

Corresponding Author

Tel.: +47 77644086. E-mail: john-sigurd.svendsen@uit.no

REFERENCES

(1) Qiu, C.; Kivipelto, M.; Strauss, von, E. Epidemiology of Alzheimer's Disease: Occurrence, Determinants, and Strategies Toward Intervention. *Dialogues. Clin. Neurosci.* **2009**, *11* (2), 111–128.

(2) Alzheimer, A. Über Einen Eeigenartigen Schweren Erkrankungsprozeß Der Hirnrinde. *Neurologisches Centralblatt* **1906**, *23*, 1129–1136.

(3) Hardy, J. A.; Higgins, G. A. Alzheimer's Disease: the Amyloid Cascade Hypothesis. *Science* **1992**, *256* (5054), 184–185.

(4) Mazanetz, M. P.; Fischer, P. M. Untangling Tau Hyperphosphorylation in Drug Design for Neurodegenerative Diseases. *Nat. Rev. Drug Discov.* **2007**, *6* (6), 464–479.

(5) Querfurth, H. W.; LaFerla, F. M. Alzheimer's Disease. *N. Engl. J. Med.* **2010**, *362* (4), 329–344.

(6) Chételat, G. Alzheimer Disease: Aβ-Independent Processes—Rethinking Preclinical AD. *Nat. Rev. Neurol.* **2013**, *9* (3), 123–124.

(7) Giacobini, E.; Gold, G. Alzheimer Disease Therapy--Moving From Amyloid-β to Tau. *Nat. Rev. Neurol.* **2013**, *9* (12), 677–686.

(8) Medina, M.; Avila, J. New Perspectives on the Role of Tau in Alzheimer's Disease. Implications for Therapy. *Biochem. Pharmacol.* **2014**, *88* (4), 540–547.

(9) Drachman, D. A. The Amyloid Hypothesis, Time to Move on: Amyloid Is the Downstream Result, Not Cause, of Alzheimer's Disease. *Alzheimers Dement.* **2014**, *10* (3), 372–380.

(10) Wischik, C. M.; Harrington, C. R.; Storey, J. M. D. Tau-Aggregation Inhibitor Therapy for Alzheimer's Disease. *Biochem. Pharmacol.* **2014**, *88* (4), 529–539.

(11) Lewis, J.; McGowan, E.; Rockwood, J.; Melrose, H.; Nacharaju, P.; Van

Slegtenhorst, M.; Gwinn-Hardy, K.; Paul Murphy, M.; Baker, M.; Yu, X.; Duff, K.; Hardy, J.; Corral, A.; Lin, W. L.; Yen, S. H.; Dickson, D. W.; Davies, P.; Hutton, M. Neurofibrillary Tangles, Amyotrophy and Progressive Motor Disturbance in Mice Expressing Mutant (P301L) Tau Protein. *Nat. Genet.* **2000**, *25* (4), 402–405.

(12) Wang, Y.; Mandelkow, E. Tau in Physiology and Pathology. *Nat. Rev. Neurosci.* **2015**.

(13) Lloret, A.; Fuchsberger, T.; Giraldo, E.; Viña, J. Molecular Mechanisms Linking Amyloid B Toxicity and Tau Hyperphosphorylation in Alzheimer′S Disease. *Free Radic. Biol. Med.* **2015**, *83*, 186–191.

(14) Wegiel, J.; Gong, C.-X.; Hwang, Y.-W. The Role of DYRK1A in Neurodegenerative Diseases. *FEBS J.* **2011**, *278* (2), 236–245.

(15) Smith, B.; Medda, F.; Gokhale, V.; Dunckley, T.; Hulme, C. Recent Advances in the Design, Synthesis, and Biological Evaluation of Selective DYRK1A Inhibitors: a New Avenue for a Disease Modifying Treatment of Alzheimer's? *ACS Chem. Neurosci.* **2012**, *3* (11), 857–872.

(16) Wegiel, J.; Kaczmarski, W.; Barua, M.; Kuchna, I.; Nowicki, K.; Wang, K.-C.; Wegiel, J.; Yang, S. M.; Frackowiak, J.; Mazur-Kolecka, B.; Silverman, W. P.; Reisberg, B.; Monteiro, I.; de Leon, M.; Wisniewski, T.; Dalton, A.; Lai, F.; Hwang, Y.-W.; Adayev, T.; Liu, F.; Iqbal, K.; Iqbal, I.-G.; Gong, C.-X. Link Between DYRK1A Overexpression and Several-Fold Enhancement of Neurofibrillary Degeneration with 3-Repeat Tau Protein in Down Syndrome. *J. Neuropathol. Exp. Neurol.* **2011**, *70* (1), 36–50.

(17) Ryoo, S.-R.; Jeong, H. K.; Radnaabazar, C.; Yoo, J.-J.; Cho, H.-J.; Lee, H.-W.; Kim, I.-S.; Cheon, Y.-H.; Ahn, Y. S.; Chung, S.-H.; Song, W.-J. DYRK1A-Mediated Hyperphosphorylation of Tau - a Functional Link Between Down Syndrome and

Alzheimer Disease. *J. Biol. Chem.* **2007**, *282* (48), 34850–34857.

(18) Berg, S.; Bergh, M.; Hellberg, S.; Högdin, K. Discovery of Novel Potent and Highly Selective Glycogen Synthase Kinase-3β (GSK3β) Inhibitors for Alzheimer's Disease: Design, Synthesis, and Characterization of Pyrazines. *J. Med. Chem.* **2012**, *55* (21), 9107–9119.

(19) Becker, W.; Sippl, W. Activation, Regulation, and Inhibition of DYRK1A. *FEBS J.* **2011**, *278* (2), 246–256.

(20) Ferrer, I.; Gomez-Isla, T.; Puig, B.; Freixes, M.; Ribe, E.; Dalfo, E.; Avila, J. Current Advances on Different Kinases Involved in Tau Phosphorylation, and Implications in Alzheimers Disease and Tauopathies. *Curr. Alzheimer Res.* **2005**, *2* (1), 3–18.

(21) Song, W.-J.; Song, E.-A. C.; Choi, S.-H.; Baik, H.-H.; Jin, B. K.; Kim, J. H.; Chung, S.-H. Dyrk1A-Mediated Phosphorylation of RCAN1 Promotes the Formation of Insoluble RCAN1 Aggregates. *Neurosci. Lett.* **2013**, *554*, 135–140.

(22) Jung, M.-S.; Park, J.-H.; Ryu, Y. S.; Choi, S.-H.; Yoon, S.-H.; Kwen, M.-Y.; Oh, J. Y.; Song, W.-J.; Chung, S.-H. Regulation of RCAN1 Activity by DYRK1A-Mediated Phosphorylation. *J. Biol. Chem.* **2011**, *286* (46), 40401–40412.

(23) Walte, A.; Rüben, K.; Birner-Gruenberger, R.; Preisinger, C.; Bamberg-Lemper, S.; Hilz, N.; Bracher, F.; Becker, W. Mechanism of Dual Specificity Kinase Activity of DYRK1A. *FEBS J.* **2013**, *280* (18), 4495–4511.

(24) Ryu, Y. S.; Park, S. Y.; Jung, M.-S.; Yoon, S.-H.; Kwen, M.-Y.; Lee, S. Y.; Choi, S.-H.; Radnaabazar, C.; Kim, M.-K.; Kim, H.; Kim, K.; Song, W.-J.; Chung, S.-H. Dyrk1A-Mediated Phosphorylation of Presenilin 1: a Functional Link Between Down Syndrome and Alzheimer's Disease. *J. Neurochem.* **2010**, *115* (3), 574–584.

(25) Ryoo, S. R.; Cho, H. J.; Lee, H. W.; Jeong, H. K.; Radnaabazar, C.; Kim, Y. S.; Kim, M. J.; Son, M. Y.; Seo, H.; Chung, S. H. Dual-Specificity Tyrosine (Y)-

Phosphorylation Regulated Kinase 1A-Mediated Phosphorylation of Amyloid Precursor Protein: Evidence for a Functional Link Between Down Syndrome and Alzheimer's Disease. *J. Neurochem.* **2008**, *104* (5), 1333–1344.

(26) Brunden, K. R.; Trojanowski, J. Q.; Lee, V. M. Y. Advances in Tau-Focused Drug Discovery for Alzheimer's Disease and Related Tauopathies. *Nat. Rev. Drug Discov.* **2009**, *8* (10), 783–793.

(27) Becker, R. E.; Greig, N. H.; Giacobini, E.; Schneider, L. S.; Ferrucci, L. A New Roadmap for Drug Development for Alzheimer's Disease. *Nat. Rev. Drug Discov.* **2014**, *13* (2), 156–156.

(28) Becker, W.; Soppa, U.; Tejedor, F. DYRK1A: a Potential Drug Target for Multiple Down Syndrome Neuropathologies. *CNS Neurol. Disord. Drug Targets* **2013**, *13* (1), 26–33.

(29) Rothweiler, U.; Eriksson, J.; Stensen, W.; Leeson, F.; Engh, R. A.; Svendsen, J. S. Luciferin and Derivatives as a DYRK Selective Scaffold for the Design of Protein Kinase Inhibitors. *Eur. J. Med. Chem.* **2015**, *94*, 140–148.

(30) Stuckwisch, C. G. Derivatives of 2-Amino-6-Methoxybenzothiazole. *J. Am. Chem. Soc.* **1949**, *71* (10), 3417–3417.

(31) Graczyk, P. P. Gini Coefficient: a New Way to Express Selectivity of Kinase Inhibitors Against a Family of Kinases. *J. Med. Chem.* **2007**, *50* (23), 5773–5779.

(32) Hopkins, A. L.; Groom, C. R.; Alex, A. Ligand Efficiency: a Useful Metric for Lead Selection. *Drug Discov. Today* **2004**, *9* (10), 430–431.

(33) Ogawa, Y.; Nonaka, Y.; Goto, T.; Ohnishi, E.; Hiramatsu, T.; Kii, I.; Yoshida, M.; Ikura, T.; Onogi, H.; Shibuya, H.; Hosoya, T.; Ito, N.; Hagiwara, M. Development of a Novel Selective Inhibitor of the Down Syndrome-Related Kinase Dyrk1A. *Nat. Commun.* **2010**, *1*, 86.

(34) Alexeeva, M.; Åberg, E.; Engh, R. A.; Rothweiler, U. The Structure of a Dual-Specificity Tyrosine Phosphorylation-Regulated Kinase 1A-PKC412 Complex Reveals Disulfide-Bridge Formation with the Anomalous Catalytic Loop HRD(HCD) Cysteine. *Acta Crystallogr. D Biol. Crystallogr.* **2015**, *71* (Pt 5), 1207–1215.

(35) Natarajan Kannan, A. F. N. Evolutionary Constraints Associated with Functional Specificity of the CMGC Protein Kinases MAPK, CDK, GSK, SRPK, DYRK, and CK2α. *Protein Sci.* **2004**, *13* (8), 2059–2077.

(36) Zhou, P.; Zou, J.; Tian, F.; Shang, Z. Fluorine Bonding - How Does It Work in Protein-Ligand Interactions? *J. Chem. Inf. Model.* **2009**, *49* (10), 2344–2355.

(37) Bissantz, C.; Kuhn, B.; Stahl, M. A Medicinal Chemist's Guide to Molecular Interactions. *J. Med. Chem.* **2010**, *53* (14), 5061–5084.

(38) Paulini, R.; Muller, K.; Diederich, F. Orthogonal Multipolar Interactions in Structural Chemistry and Biology. *Angew. Chem. Int. Edit.* **2005**, *44* (12), 1788–1805.

(39) Mooibroek, T. J.; Gamez, P. Halogen ... Phenyl Supramolecular Interactions in the Solid State: Hydrogen Versus Halogen Bonding and Directionality. *Crystengcomm* **2013**, *15* (9), 1802–1805.

(40) Daeffler, K. N.-M.; Lester, H. A.; Dougherty, D. A. Functionally Important Aromatic-Aromatic and Sulfur-Π Interactions in the D2 Dopamine Receptor. *J. Am. Chem. Soc.* **2012**, *134* (36), 14890–14896.

(41) Jeffrey, G. A. *An Introduction to Hydrogen Bonding*; Oxford University Press: Oxford, 1997.

(42) Krug, M.; Weiss, M. S.; Heinemann, U.; Mueller, U. XDSAPP: a Graphical User Interface for the Convenient Processing of Diffraction Data Using XDS. *J. Appl. Crystallogr.* **2012**, *45* (3), 568–572.

(43) Kabsch, W. Xds. *Acta Crystallogr. D Biol. Crystallogr.* **2010**, *66* (Pt 2), 125–132.

(44) McCoy, A. J.; Grosse-Kunstleve, R. W.; Adams, P. D.; Winn, M. D.; Storoni, L. C.; Read, R. J.; IUCr. Phaser Crystallographic Software. *J. Appl. Crystallogr.* **2007**, *40* (4), 658–674.

(45) Adams, P. D.; Afonine, P. V.; Bunkóczi, G.; Chen, V. B.; Davis, I. W.; Echols, N.; Headd, J. J.; Hung, L.-W.; Kapral, G. J.; Grosse-Kunstleve, R. W.; McCoy, A. J.; Moriarty, N. W.; Oeffner, R.; Read, R. J.; Richardson, D. C.; Richardson, J. S.; Terwilliger, T. C.; Zwart, P. H. PHENIX: a Comprehensive Python-Based System for Macromolecular Structure Solution. *Acta Crystallogr. D Biol. Crystallogr.* **2010**, *66* (Pt 2), 213–221.

(46) Winn, M. D.; Ballard, C. C.; Cowtan, K. D.; Dodson, E. J.; Emsley, P.; Evans, P. R.; Keegan, R. M.; Krissinel, E. B.; Leslie, A. G. W.; McCoy, A.; McNicholas, S. J.; Murshudov, G. N.; Pannu, N. S.; Potterton, E. A.; Powell, H. R.; Read, R. J.; Vagin, A.; Wilson, K. S. Overview of the CCP4 Suite and Current Developments. *Acta Crystallogr. D Biol. Crystallogr.* **2011**, *67* (Pt 4), 235–242.

(47) Murshudov, G. N.; Skubak, P.; Lebedev, A. A.; Pannu, N. S.; Steiner, R. A.; Nicholls, R. A.; Winn, M. D.; Long, F.; Vagin, A. A. REFMAC5 for the Refinement of Macromolecular Crystal Structures. *Acta Crystallogr. D Biol. Crystallogr.* **2011**, *67* (Pt 4), 355–367.

(48) Emsley, P.; Lohkamp, B.; Scott, W. G.; Cowtan, K.; IUCr. Features and Development of Coot. *Acta Crystallogr. D Biol. Crystallogr.* **2010**, *66* (4), 486–501.

(49) Schuttelkopf, A. W.; van Aalten, D. PRODRG: a Tool for High-Throughput Crystallography of Protein-Ligand Complexes. *Acta Crystallogr. D Biol. Crystallogr.* **2004**, *60* (Pt 8), 1355–1363.

(50) Singh, P.; Harden, B. J.; Lillywhite, B. J.; Broad, P. M. Identification of Kinase Inhibitors by an ATP Depletion Method. *Assay. Drug Dev. Technol.* **2004**, *2* (2),

161–169.

(51) Hastie, C. J.; McLauchlan, H. J.; Cohen, P. Assay of Protein Kinases Using Radiolabeled ATP: a Protocol. *Nat. Protc.* **2006**, *1* (2), 968–971.

TOC graphics